Characterization of clays used in the ceramic manufacturing industry by reflectance spectroscopy: An experiment in the São Simão ball-clay deposit, Brazil

Juliano Alves de Senna, Carlos Roberto de Souza Filho *, Rômulo Simões Angélica

Geosciences Institute, University of Campinas, PO Box 6152, 13083-970, Campinas, Sao Paulo, Brazil

Abstract

The characterization of clays from the physical, chemical, and ceramic standpoint in pre-and-within mining stages is a necessary step. However, succinct mining planning, lack of industry-oriented standards and the usual bond to empirical discrimination of clays as regards their use, imply in mixing chemically and technologically different materials, with serious consequences to the mining and manufacturing process. Taking the alluvium-derived, ball-clay deposit of São Simão (SS) as a case study, this works aims to evaluate the potential of reflectance spectroscopy (RS) as a method to define types, purity and crystallinity of clays and to seek a possible relation between spectral characteristics of clays and their use in the ceramic industry. The SS deposit hosts three types of clays that were spectrally set apart based on RS. The technique indicated that the white clays comprise highly ordered kaolinite, mica, smectite and lepidocrosite (first finding in Brazilian alluviums). The brown clays are also rich in well-ordered kaolinite and contain abundant Fe-bearing minerals, as goethite, hematite and siderite (rarely found in alluviums). The gray clays are kaolinite-poor and are abundant in organic matter and smectites. Each of the clay classes typified in the SS deposit has a specific application in the fine ceramic industry, indicating the prominent potential of RS to characterize industrial materials.
© 2007 Elsevier B.V. All rights reserved.

1. Introduction

The São Simão (SS) ball-clay deposit comprises a very important type of clay used in the Brazilian ceramic industry, as it comprises one of few sources in the country for manufacturing porcelain and pottery of superior quality. These clays are fine-grained (<2 µm), rich in "hexagonal" kaolinite but also contain smectites, mica

adsorbed to kaolinite crystal faces (Pressinotti, 1991) and organic matter. The SS clays are characterized by their high plasticity, resistance under dry conditions, extensive thermal vitrification and light burning color under heating (Wilson, 1983; Santos, 1992). The deposit is located in the northeastern region of the São Paulo State, Brazil, about 8 km west of the São Simão town (Fig. 1).

Despite the unique features of the SS clays, their characterization from the physical, chemical, and ceramic standpoint in pre-and-within mining stages is a difficult task. Considering the intrinsic complexities

* Corresponding author.
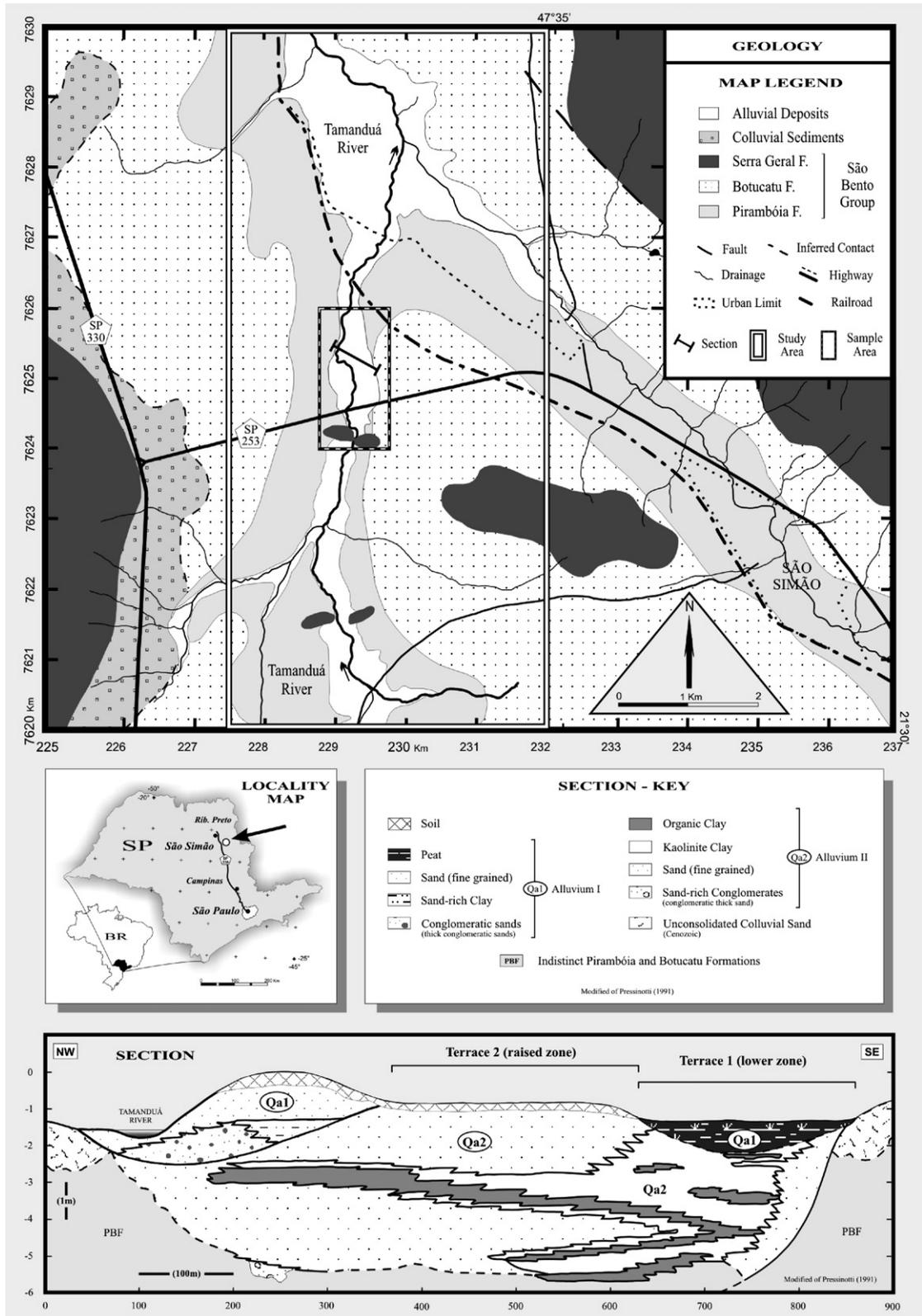*E-mail address:* beto@ige.unicamp.br (C.R. de Souza Filho).

Fig. 1. Locality map and geological setting of the study area.

involved in characterizing clays by conventional methods (i.e., specifics on sample preparation), this works aims (i) to evaluate the potential of reflectance spectroscopy as a complementary, expedite and portable method to characterize clays, including definition of their type, composition and crystallinity, and (ii) to study the possibility to relate clays classified on the basis of their spectral characteristics to specific uses in the ceramic industry, using the SS deposit as a case study.

2. Reflectance spectroscopy–background

Spectroscopy is a tool that has been used for decades to identify, understand, and quantify solid, liquid or gaseous materials, especially in the laboratory. In several disciplines, spectroscopic measurements are used to detect absorption features due to specific chemical bonds, and detailed analyses are used to determine the abundance and physical state of the detected absorbing species (Clark, 1999). Visible and infrared reflectance spectroscopy (RS), in particular, is a key tool used in remote sensing sciences (Sabins, 1999; Drury, 2001) and it is a sensitive method in detecting clay minerals in the shortwave infrared range (SWIR : 1.3–2.5 μm) of the electromagnetic spectrum. This is a fast, non-destructive and operational method that can be applied in mineral determination and mapping (Hunt, 1977, 1980). RS of natural surfaces are sensitive not only to specific chemical bonds in materials, but also has the advantage of being sensitive to both high and low ordered crystalline materials. It aims to measure, along different and continuous wavelengths, the amount of radiation reflected by the surface of materials, which is displayed as reflectance spectra. Absorption features in the spectra of minerals are due to the presence of specific molecular groups and, depending on wavelength position, shape and intensity, can be often used to diagnose minerals present in a sample, providing clues on their relative proportion and abundance (Clark, 1999).

With the advent of portable, high resolution spectrometers (Gladwell et al., 1983), RS has been widely used both to support studies about the complexities involved in energy-matter interaction, that forms the basis of remote sensing studies (Curtiss and Goetz, 1994; Kruse, 1997), and to aid mineral identification and crystallography investigations (Goetz et al., 1991; Taylor et al., 1997; Martinez-Alonso et al., 2002a,b).

A major advantage of RS over other analytical methods (X-ray powder diffraction; mid-infrared (MIR, 2.5–25 mm) infrared transmission spectroscopy), is that reflectance measurements usually can be made without any sample preparation and grinding. For clay minerals this is particular important as the grinding of samples to prepare extremely fine material for dispersion can imply in structural damage and alter the analytical result. Care must also be taken to use RS on powdered materials. In relatively transparent materials, light is scattered out of fine-grained samples before much absorption takes place, resulting in spectra that have weak absorption bands and a bright background or "continuum". Relatively coarser samples commonly show more pronounced absorption bands (Crowley and Vergo, 1988).

3. Geological setting of the São Simão deposit

The geology around the SS deposit (Fig. 1) comprises lithostratigraphic units of the Paleozoic–Mesozoic São Bento Group (sedimentary rocks of the Pirambóia and Botucatu Formations and basalts of the Serra Geral Formation), and Cenozoic sediments. The Tamanduá river (Fig. 1) occupies a N/S-trending open valley, formed in Mesozoic sediments. This valley hosts a fluvial system filled by alluvial sediments. Sediment deposition started some 30,000 years ago (Turcq et al., 1997).

Basaltic dykes and sills restrain the morphology of the river, whereas the floodplain shows two distinct terraces: terrace 1-the actual level of the river, corresponding to a lower terrace; terrace 2-an earlier, higher terrace (Fig. 1) (Pressinotti, 1991; Tanno et al., 1994). Terrace 2 is a 8 m-thick sequence made up of conglomerates at the base, followed by a thick bed of sandstones at the top, which are intercalated with turfaceous (peat) and clay-rich layers (Ruiz, 1990). In the latter, clays are concentrated in lenticular bodies up to 2 m thick (Tanno et al., 1994). These layers are vertically discontinuous, but can be laterally correlated (Pressinotti, 1991). The SS ball-clay deposit corresponds to these lenses and comprises mainly fine grained kaolinites displaying a bi-modal granulometric distribution (Tanno et al., 1994) (Fig. 1).

The clays were formed during the Late Pleistocene, between 10,000–20,000 years ago (Turcq et al., 1997). Paleohydrological studies indicate clay deposition in two stages (wet and dry periods), intercalated by erosive episodes (Pressinotti, 1991).

4. Materials and methods

Field work was aimed at collecting a large number of samples in the study area. Among 28 samples collected in the field, three main classes comprising white (WC), brown (BC) and gray (GC) clays were identified considering distinct color,
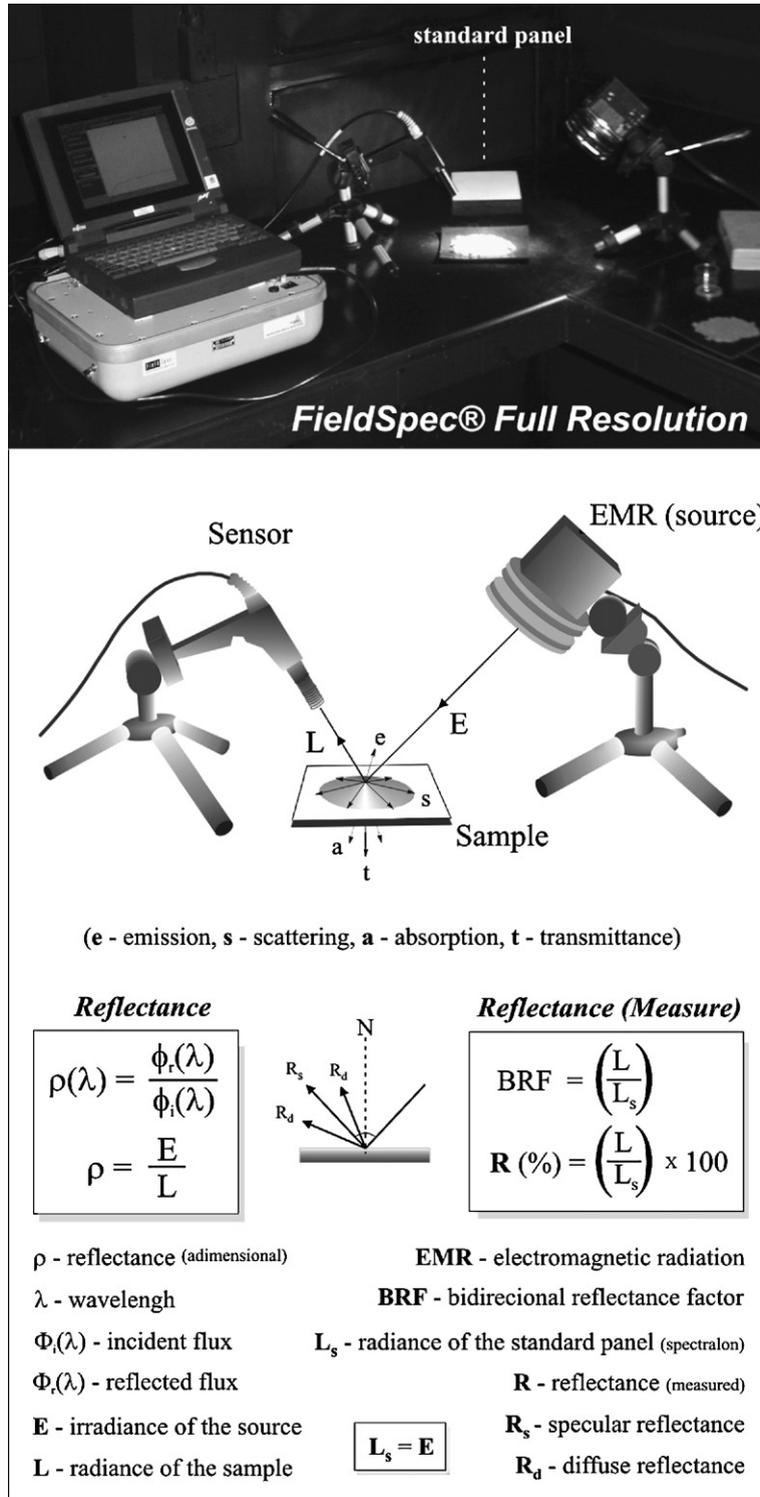
Fig. 2. General setting for lab measurements with the FieldSpec Full Resolution instrument (top figure) and schematic representation of parameters involved in such measurements.

texture, probable composition, infrared spectral features, among others aspects.

RS measurements were performed with a FieldSpec® Full Resolution spectroradiometer (Analytical Spectral Devices, Inc) (Fig. 2). This instrument offers superior signal-enhancing features, high resolution (3 nm @ 0.7 μm; 10 nm @ 1.4/ 2.1 μm), and dense sampling interval (1.4 nm @ 0.35–1.050 μm ; 2 nm @ 1.0–2.5 μm nm) within the 0.35–2.5 μm spectral range (Hatchell, 1999).

The reflectance (R), which in fact is the bidirectional reflectance factor (BRF), is expressed in percentage and comprises the ratio between the radiance (L) yielded by the sample and the radiance yielded by a Spectralon panel (Ls) (i.e., a reflectance standard that gives the highest diffuse reflectance of any known material or coating and exhibits highly lambertian behavior—its reflectance is higher than 99% for wavelengths from 0.4 μm to 1.5 μm, and higher than 95% from 1.5 μm to 2.5 μm region of the spectrum) (Fig. 2)
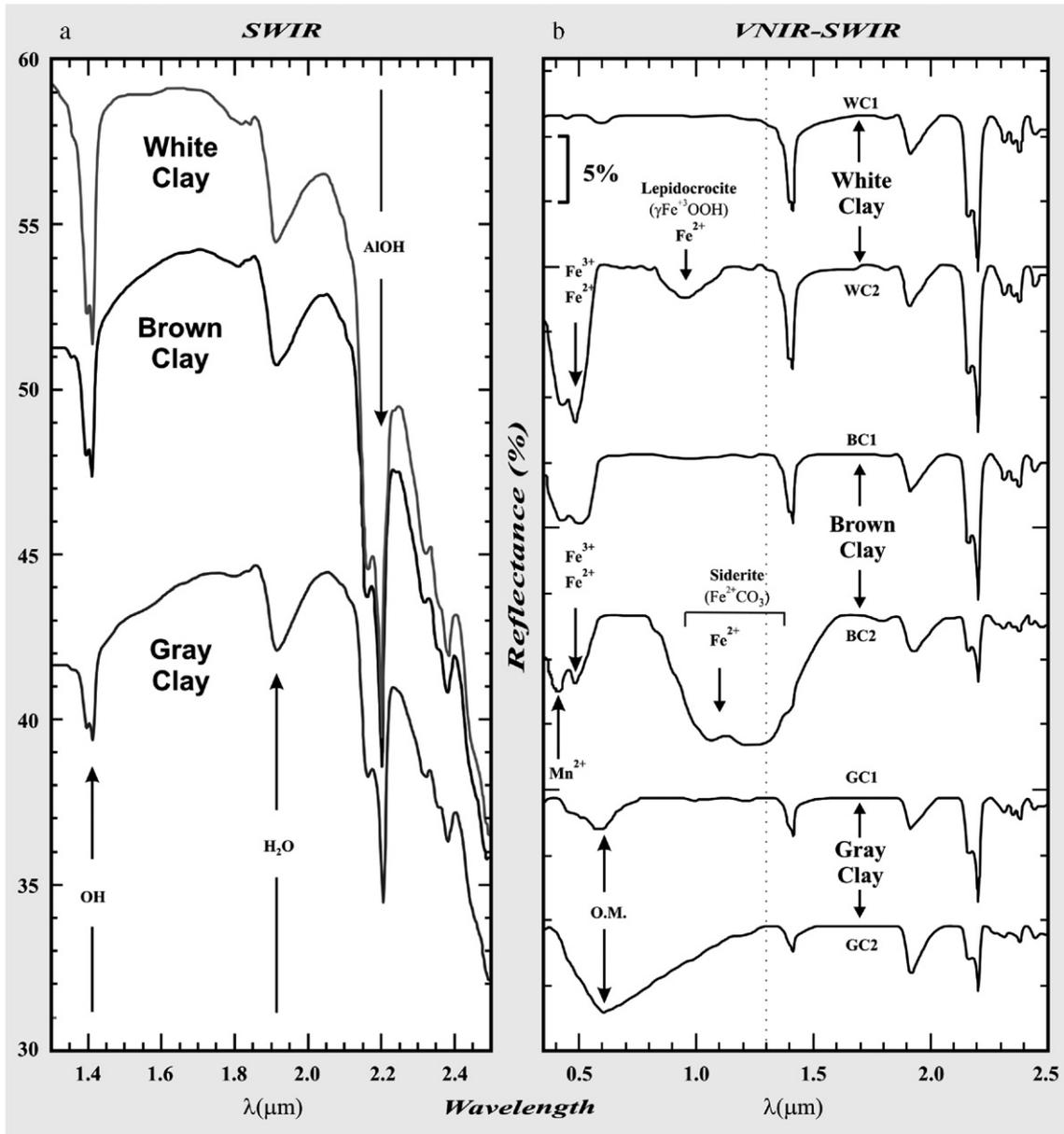

Fig. 3. (a) Absolute reflectance spectra of SS clays (white, brown and gray), in the SWIR region. (b) Relative (continuum removed and stacked) reflectance spectra of SS clays — white (WC1, WC2), brown (BC1, BC2) and gray (GC1, GC2) species, throughout the VNIR-SWIR region. O.M. = organic matter.
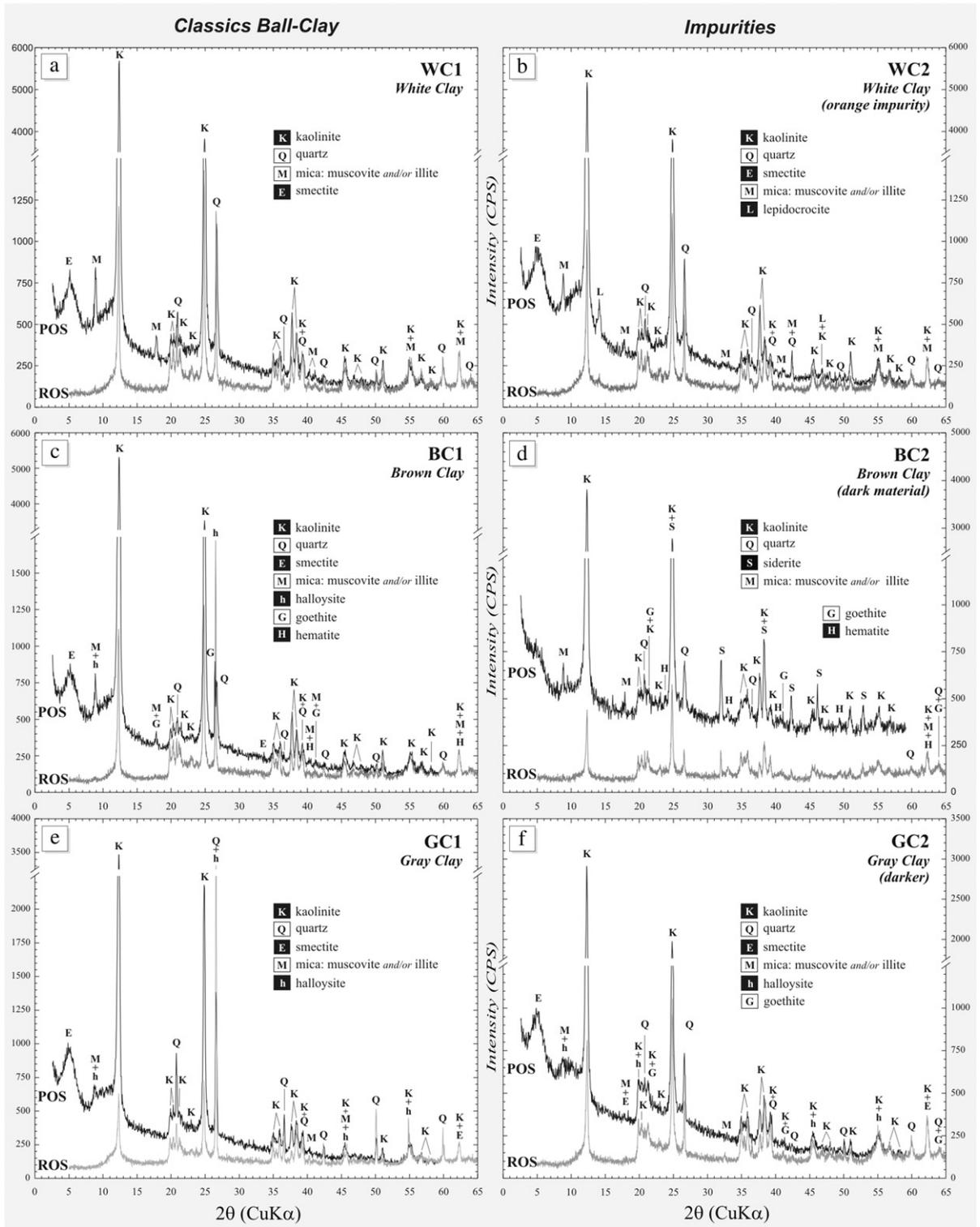
Fig. 4. X-ray diffraction patterns of white (WC), brown (BC) and gray (GC) clays. Diffractograms: POS (partly oriented samples) and ROS (randomly oriented samples).

(Crowley and Vergo, 1988; Maracci, 1992; Meneses and Madeira Netto, 2001).

Measurements were accomplished in two stages. Firstly, raw samples collected in the field were submitted to several types of readings, depending on the diversity of materials involved. This was followed by readings of coarsely crushed samples. Crushed samples stemmed from an integral part of a raw sample or from a specific portion of it, where a particular material was identified. In order to obtain a standard spectrum for each class of clay, the arithmetic mean of their respective spectral readings was computed.

Spectral-mineral classification comprised two steps: (i) spectra were classified based on SWIR (1.4–2.5 μm) (Fig. 3a) features only; and (ii) using features depicted in the complete VIS–SWIR (0.35–2.5 μm) (Fig. 3b) interval. This allowed better results for detection of clays poor in iron phases (SWIR-only), whereas the VIS–SWIR was useful to distinct between samples containing Fe-bearing minerals.

The characterization of these clays in laboratory was carried out also with the aid of powder X-ray diffraction (XRD) analysis. Samples were prepared in two different ways: totally random and partly oriented (i.e., with preferred orientation). The objective here was to establish the necessary parameters for qualitative and semi-quantitative discrimination between samples. Using XRD results, it was possible to approximate the modal composition of samples considered as representatives of each class. The XRD analysis of partially oriented samples (POS, Fig. 4) were carried out in a Siemens Diffraktometer Kristalloflex D5000 equipment, with Kα1Co (λCoKα1 = 1.7889 Å) radiation under 35 kV (power in the tube) and 25 mA (current in the filament). Samples were scanned from 3–70° (2θ) with 0.05° steps per 0.8 s. XRD of

the randomly oriented samples (ROS, Fig. 4) were carried out in a PW 3710 diffractometer with Cu anode (45 kV, 40 MA and CuKα1 radiation −1.5406 Å), divergence slit 1°, reception slit 0,2 mm, graphite monochromator, with 2θ range of 5–65° in steps of 0.02°. Samples scanned with Co radiation were converted to Cu in order to match the different patterns in the same figure. Interpretation of the diffractograms was carried out using the appropriate criteria (Brindley and Brown, 1984) with the aid of the PDF 2 (Powder Diffraction File) data base of the ICDD (International Centre for Diffraction Data).

The term "cristallinity" will be used in this paper according to recommendations of the AIPEA report (Guggenheim et al., 2006), i.e. "the degree of perfection of translational periodicity as determined by some experimental method, where diffraction techniques are the common methodologies to ascertain periodicity". Therefore, the term "kaolinite cristallinity" is referred here as the estimation of octahedral vacancy (structural) disorder in kaolinite.

The study of kaolinite crystallinity based both on RS and XRD was approached as follows:

(i) The raw reflectance spectra were first submitted to continuum removal (or hull correction) and transformed to relative reflectance. This correction involves multiplying by 100 the value given by dividing the reflectance value for each wavelength on the spectrum by the reflectance value for the same wavelength on a calculated hull line (a baseline that touches the maximum number of points on the spectrum whilst remaining convex and not crossing the spectrum line) (Pontual et al., 1997). From the relative reflectance spectra, the kaolinite diagnostic doublet centered
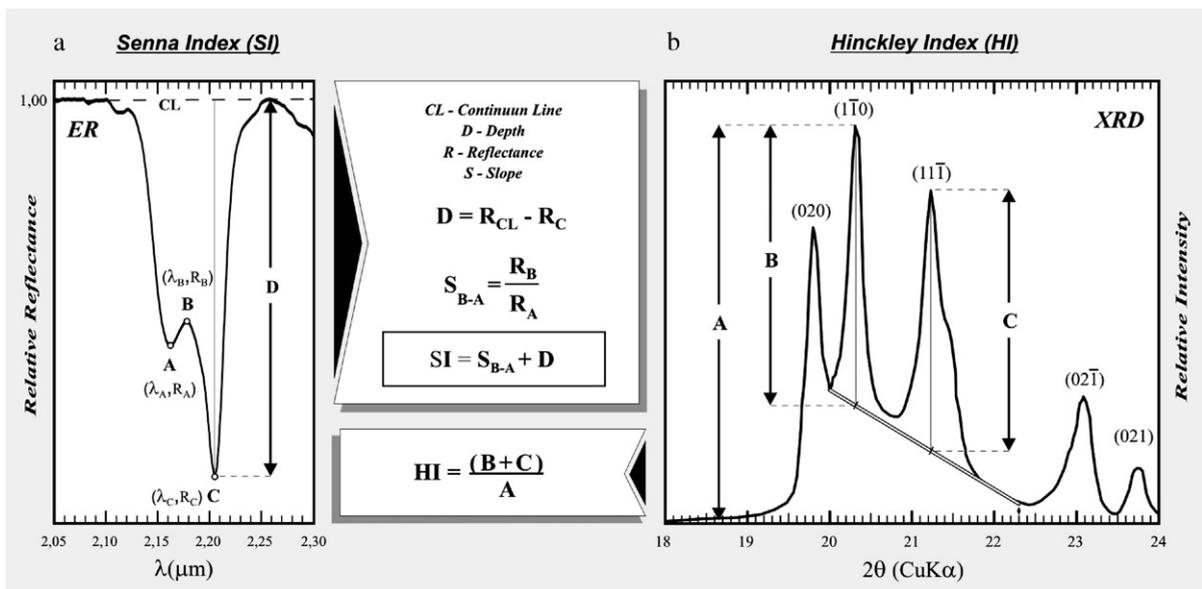

Fig. 5. Proposed schema for cristallinity evaluation. (a) Senna Index calculation based on reflectance features at 2.2 mm. (b) HI calculation based on kaolinite peaks analysis (K2 e K3 — Table 1) (modified after Plançon et al., 1988).

between 2.05 µm and 2.30 µm was extracted. Using this interval, the depth (D) of the 2.206 µm feature and the gradient (SB-A) between the reflectance at 2.162 µm and 2.180 µm were calculated (Fig. 5). These two variables were then summed to yield the Senna (kaolinite crystallinity) Index (SI) (Fig. 5). This index has advantages over previously proposed kaolinite crystallinity indices (Pontual et al., 1997; Ducart et al., 2006), as it combines not only the slope of the kaolinite features between 2.180 µm and 2162 µm (higher gradient values imply in higher crystallinity), but simultaneously measure the depth of the 2.2 µm feature (increasing depth of this feature is akin to increasing crystallinity).

(ii) The "Hinckley Index", that differentiates kaolinite samples containing ''low'' amounts of defects ('low-defect kaolinite') vs. ''high'' amounts of defects ('high-defect kaolinite') (Guggenheim et al., 2006) was also evaluated in the 18–24° (2θ) range using the non-oriented samples, according to the procedures described by Hinckley (1963) and Plançon et al. (1988) (Fig. 5). Powder difractograms were previously treated with background removal and FFT filter smoothing. HI values were yielded based on the classic region of the difractogram where a line tangent to the spectrum is positioned between the depressions at 20° (2θ) and 22.3° (2θ).

5. Results-reflectance spectroscopy and XRD

5.1. Mineralogical composition

RS analysis of SWIR absorption features (1.3–2.5 µm) (Fig. 3a), revealed a number of different spectral characteristics between the three clays. The inspection of absolute reflectance spectra for each endmember showed that the WC has stronger absorption features around 2.2 µm, followed by BC and GC. The shape (sharpness) and gradient of the 1.4 and 2.2 µm absorption features are also indicative that the WC are more crystalline specimens, due to the intensity and inflection of the doublet centered around these wavebands. Moreover, the combined appearance of the 1.4 µm and 1.8 µm features, as observed for the WC, are reliable indicators of its higher crystallinity (Pontual et al., 1997). Although the GC contains more smectites and organic matter than the other clay types, which usually imply in attenuation of spectral features by the latter, the ubiquitous presence of kaolinite sustains a clear doublet at 2.2 µm (Fig. 3a). The use of the full spectrum (0.35–2.5 µm) (Fig. 3b), including VIS–NIR wavelengths (0.35–1.30 µm), also allowed the distinction of these three clay types, but including the recognition of critical, iron-rich impurities.

A set of mineral endmembers identified in the spectral mineral classification of two representative samples of each clay class is displayed in Fig. 3b as stacked spectra and with the continuum removed. In this figure, sample WC2 (white clay) shows a feature at 0.95 µm that is due to the presence of Fe^{3+}-bearing lepidocrosite (Townsend, 1987; Clark et al., 1993). Sample BC2 (brown clay) shows double absorptions at 1.05–1.25 µm within an ample absorption feature related to Fe^{2+}-bearing carbonates, typical of siderite (Whitney et al., 1983). Siderite crystals are illustrated in Fig. 6. This sample also shows an absorption feature at 0.41 µm that is likely to be related to Mn^{2+}-bearing minerals (Hunt and Salisbury, 1971; Gaffey, 1987). Samples GC1 and GC2 display broad features centered at 0.6 µm that are indicative of the presence of organic matter. Samples WC2, BC1 and BC2 display an absorption feature at 0.5 µm that is representative of generic Fe-bearing minerals, which is abundant in the BCs.
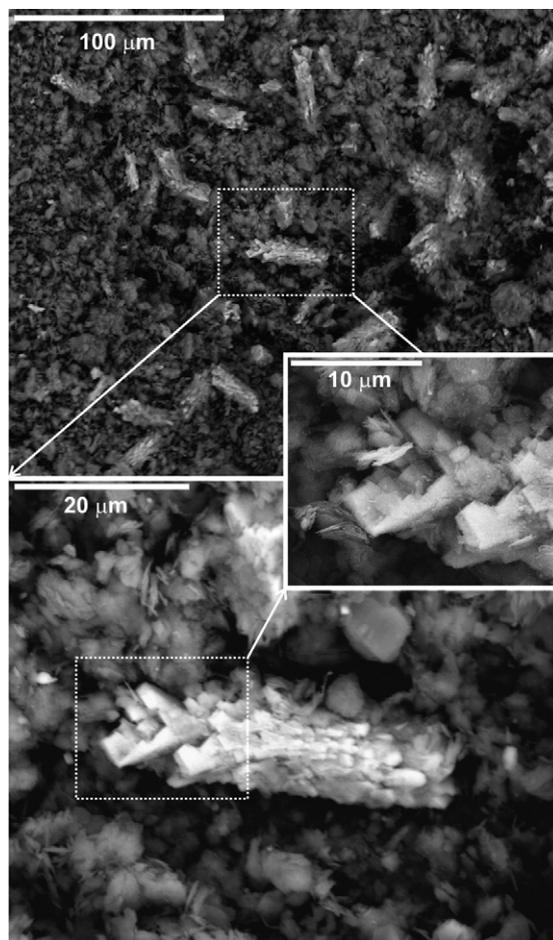

Fig. 6. SEM image of prismatic, rhombohedric siderite crystals associated with the Brown Clays.

XRD analyses showed that all clay classes are rich in kaolinite (>70%). However, considering the diffractograms and the intensity peaks K1 and K2 (Table 1), it is observed that the WC is the clay richest in kaolinite (Fig. 7), whereas the GC is kaolinite-poor. These peaks decrease from WC1 (Fig. 4a) to BC2 (Fig. 4d). Quartz is present in every class and varies between 5% (WC) to 20% (GC), approximately (see Q2 intensity-Table 1). It is abundant in sample GC1 (Fig. 4e) and scarce in BC2

Fig. 7. SEM image of typical booklets of kaolinite aggregates in the White Clays.

Table 1
Values obtained for d-spacings, hkl and relative intensity (I/Io) of the main peaks for the difractograms in Fig. 4 (hkl and intensity values are from Brindley and Brown, 1984)

PEAK	2θ (KαCu)	d (Å)	(hkl)	I/I$_0$ (%)
K^1	12.4°	7.14	001	>100
K^2 (HI)	19.9°	4.47	020	40
K^3 (HI)	20.3°	4.36	1-10	50
K^4	21.2°	4.18	11-1	50
K^5	24.9°	3.57	002	>100
K^6	35.0°	2.56	1-30/20-1	60
K^7	36.0°	2.49	1-3-1/200	80
K^8	37.8°	2.38	003	60
K^9	38.4°	2.34	1-31/20-2	90
K^{10}	39.3°	2.29	131	80
K^{11}	45.5°	1.99	20-3/1-32	60
K^{12}	51.1°	1.79	004	40
K^{13}	55.1°	1.67	20-4	70
K^{14}	62.3°	1.49	060	80
Q^1	20.9°	4.26	100	35
Q^2	26.7°	3.34	101	100
Q^3	36.5°	2.46	110	12
Q^4	39.4°	2.28	102	12
Q^5	50.1°	1.82	112	17
Q^6	59.9°	1.54	211	15
M^1	8.8°	10.0	001	>100
M^2	17.8	4.98	002	37
E	5.0°	17.6	001	100
h^1	8.8°	10.1	001	100
h^2	26.5°	3.40	003	50
H^1	33.3°	2.70	104	100
H^2	40.8°	2.21	113	23
H^3	49.4°	1.84	024	39
G^1	17.8°	4.98	020	15
G^2	21.3°	4.18	110 (11-1)	100
G^3	26.4°	3.38	120	10
G^4	41.1°	2.19	140	20
G^5	64.0°	1.45	061	10
L	14.11°	6.27	020	100
S^1	24.86°	3.58	102	25
S^2	32.05°	2.79	104	100
S^3	38.31°	2.35	110	15
S^4	42.34°	2.13	113	20
S^5	46.14°	1.97	201	15
S^6	52.89°	1.73	116	20

K = kaolinite, Q = quartz low, M = mica, E = smectite (T), h = halloysite (10 Å), H = hematite, G = goethite, L = lepidocrocite, S = siderite.
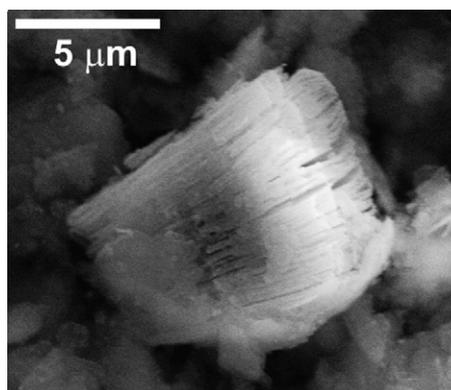
(Fig. 4d). Samples that contain fewer impurities are richer in quartz (Fig. 4). Mica contents in samples WC and BC are 10% and 5%, respectively. Mica is rare or absent in most GCs (Fig. 4e,f), as indicated by the lack of intrinsic peaks at M1 e M2 (Table 1). Smectites are found mainly in the GC (5–10%) (Fig. 4e, f) and are lacking only in sample BC2 (Fig. 4d). They are less ordered minerals as indicated by their broader peaks (E-Table 1). Halloysite (10 Å) is marked by peaks h1 e h2 (Table 1) and usually is associated with zones wealthy in organic matter. Hematite and goethite occur simultaneously (Fig. 4c, d, f and Table 1) and account for the BCs distinctive pigmentation. Lepidocrosite (~10%) occurs in orange-coloured WCs zones; it shows up mainly in the oriented samples (POS-Fig. 4b) with a characteristic peak (L-Table 1) and its signature suggests that this is a highly ordered type, possibly formed in slow oxidation conditions (Fortin et al., 1993; Sei et al., 2004). Siderite (>10%) appears within coarser and darker zones of the BCs (Fig. 4d). It is identified in the diffractograms by several archetypal planar reflections (S1–S6-Table 1). Siderite may be also present in sample WC2 (Fig. 4b), considering the display of some planar reflections (e.g., S4-Table 1) plus the fact that the quartz peak is stronger in this sample in comparison to sample WC1 (Fig. 4a).

5.2. Kaolinite crystallinity (or structural disorder)

Structural disorder in kaolinite can be the result of non-regular interlayer shifts, non-regular rotations of layers, or faults involving the position of the vacancy in the octahedral sheet (Brindley, 1980). XRD studies have demonstrated that vacancy displacements within the octahedral sheet constitute the most important type of defect (Plançon et al., 1988).
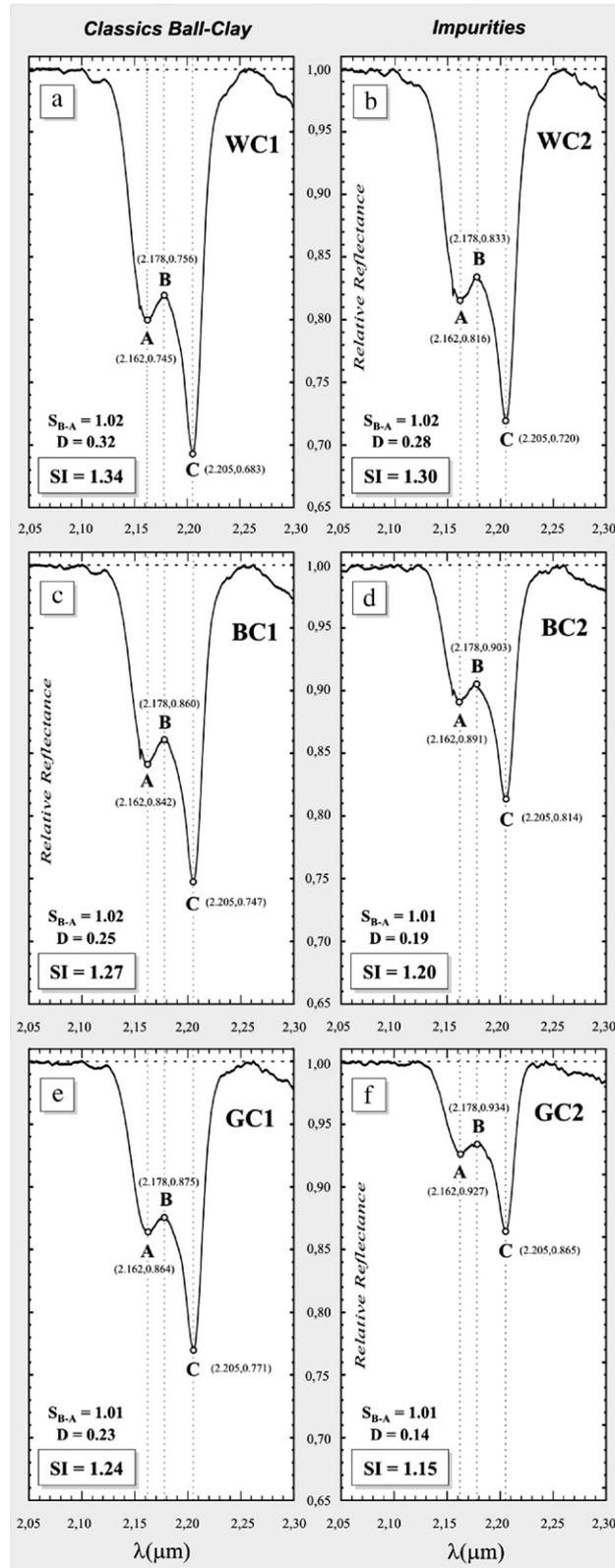
Fig. 8. SI (Senna Index) values yielded for archetypal ball-clays of the São Simão deposit, including samples containing impurities.
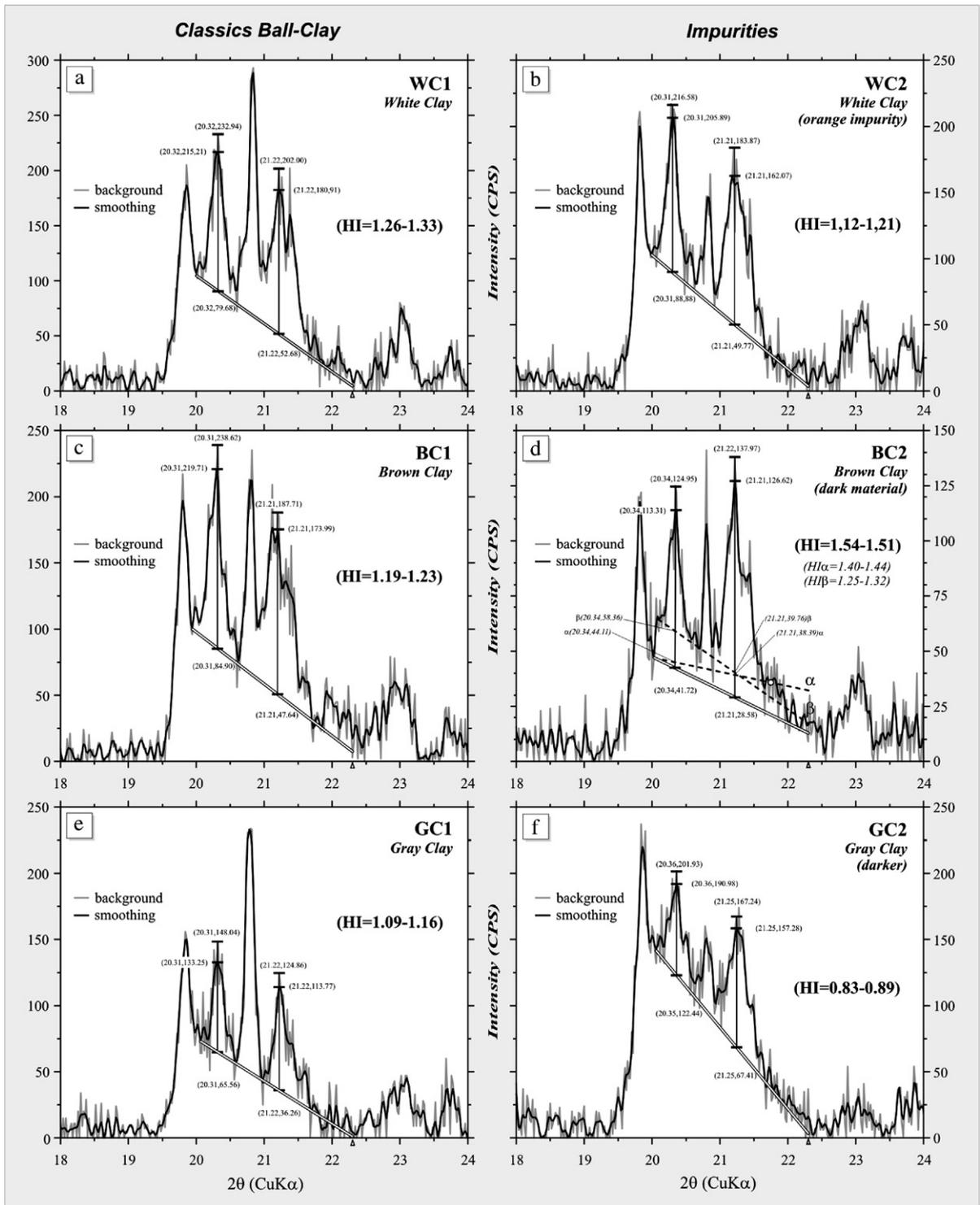
Fig. 9. HI (Hinckley Index) values yielded for archetypal ball-clays of the São Simão deposit, including samples containing impurities (b,d,f).

The approach based on RS and the SI (Fig. 5) for the estimation of structural disorder in kaolinite allowed the establishment of a gradation between poorly and well ordered kaolinites within the exemplary ball-clays of the São Simão deposit. SI values indicate an increase in crystallinity for the studied samples from well, through

moderate to poorly ordered, as follows: WC1 > WC2 > BC1 > GC1 > BC2 > GC2 (Fig. 8). WC1 (Fig. 8a) and GC2 (Fig. 8f) show SI values of 1.34 and 1.15 and, therefore, are typified as clays with the highest and lowest crystallinity within the set, respectively. Besides the higher SI values, it is interesting to note that well ordered kaolinites show steeper spectral gradients between 2.25–2.30 μm (Fig. 8) and this feature could be used additionally in the determination of relative crystallinity.

The investigation of equivalent samples involving the HI (Fig. 5) also permitted to organize the set as regards crystallinity (Fig. 9), from higher to lower, as follows: WC1 > WC2 > BC1 > GC1 > GC2. Sample BC2 (Fig. 9d), however, yielded a dissimilar and over-estimated HI value (> 1.5) than expected. Such discrepancy is maintained even for HIs computed on the basis of other criteria (HIα and HIβ) (Fig. 9d). Our analysis shows this is probably due to the combination of one of the goethite planar reflections (G2-Table 1) with another planar reflection of kaolinite (K4-Table 1).

6. Discussions

The three types of clays found in the SS deposit are spectrally distinguishable based on RS results, which substantiated and augmented the results yielded through XRD-analysis of equivalent samples. The technique indicated that: (i) WCs host greater concentration of well ordered, highly crystalline kaolinite and abundant

micas; (ii) BCs contain lower abundance of kaolinite in comparison with WCs, but show significant amounts of goethite and hematite; (iii) GCs are relatively poor in kaolinite but considerably rich in smectites and organic matter. Mineral impurities that usually inflict distinct color and texture properties to the samples are marked by lepidocrocite (WCs) and siderite (BCs). The content of goethite/hematite and organic matter also control the color appearance on BCs and GCs, respectively.

The study of kaolinite crystallinity based on RS analysis (ie., SI) discriminated the SS ball-clays successfully and showed a key hierarchy between well and poorly ordered specimens that is akin to the traditional approach based on XDR analysis (ie., HI).

Fig. 10 comprises the graphic relations between SI and HI values yielded from all the studied samples. The classic ball-clays WC1, BC1 and GC1 are positioned ascendingly in both SI versus HI and HI versus SI diagrams (Fig. 10). These diagrams uniquely show that WC1 and GC1 are the more and the less crystalline specimens, respectively. Using these diagrams is also possible to predict an adequate HI index for samples contaminated by iron hydroxides and, therefore, to account for their actual crystallinity — as is the case for sample BC2. Using the equations displayed in Fig. 10a new HI was calculated for BC2 and this showed coherency with the crystallinity predicted for this sample, which occupies a new field in the SI x HI diagram.

Considering that the standard HI range varies from 0.2 to 1.5 (Plançon et al., 1988), the high HI values
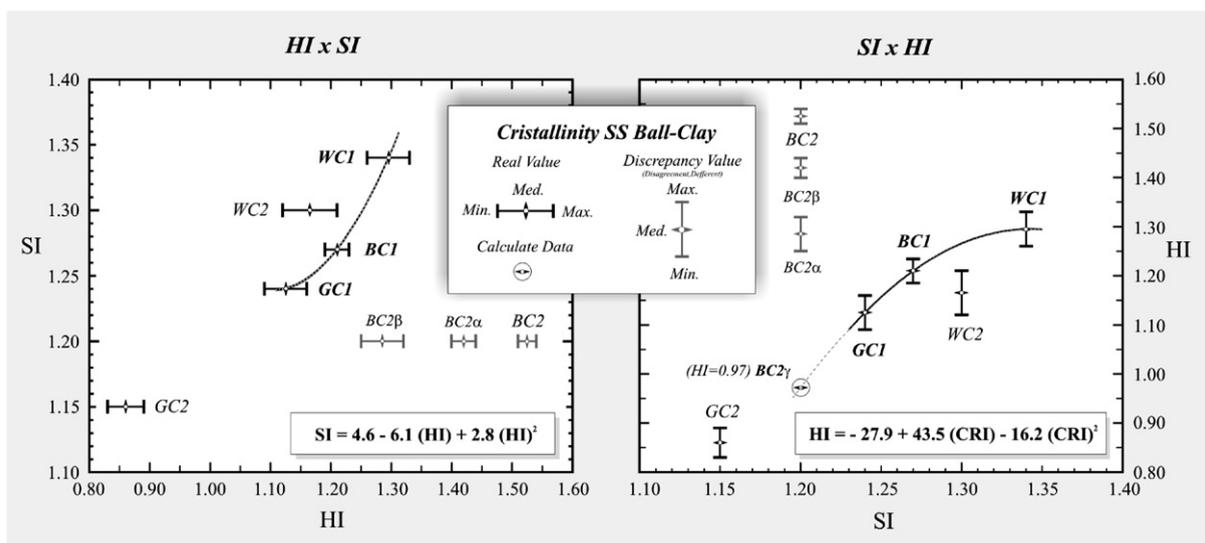

Fig. 10. Cristallinity signature of the ball-clays of the São Simão deposit considering HI vs SI and SI vs HI relationships. Equations in each diagram can be used to compensate index values biased by the presence of excessive impurities and for the recalculation of outliers.

yielded for the SS ball-clays (HI > 1.0) also substantiates their overall type as well ordered kaolinites.

Another interesting finding of this study is that each type of clays characterized by RS in the SS deposit, coincidently, showed a specific application in the ceramic industry. The WCs are considered the best quality clay product available in the SS deposit. This is sustained by the fact demonstrated through RS that these clays are highly pure and rich in crystalline kaolinite and poor in Fe-bearing stains. SS WCs are extensively used by white porcelain manufacturing industries in Brazil.

Although they do not display a white color that is typically associated with clay quality in the ceramic industry, the BCs and the GCs are of great use by sanitaryware manufacturers. These clays are known to be extremely plastic-a feature associated with the content of smectites detected by RS (BCs) and organic matter (GCs).

Therefore, our results indicate that RS analysis is a suitable method for the determination of kaolinite crystallinity. Limitations of XRD analysis are two-fold. Firstly, a particular degree of long-range ordering is essential within the kaolinite to permit detection of the XRD peaks that provide the crystallinity information (HI). Conversely, RS analysis is responsive to localized intra-layer variations that cannot simply be detected by XRD. This makes RS a lot more sensitive to subtle variations in crystallinity than XRD, as also previously indicated by Crowley and Vergo (1988) and Pontual et al. (1997). Secondly, the presence of impurities in the sample, such as iron hydroxides, imposes planar reflection interferences that also modify the crystallinity information (HI). This is another problem straightforwardly transcended by RS. Using SI values as a control, HI biased by the presence of such impurities can be corrected and more accurately elaborated using a model equation as provided in this work.

7. Conclusions

RS supported the successful characterization of three classes of clays in the SS ball-clay deposit regarding their composition, purity and crystallinity. In laboratory, XRD analysis carried out on the same samples confirmed the obtained results. This indicates that RS analysis can be utilized as a portable method in the field for clay classification.

The occurrence of lepidocrocite (first finding in Brazilian alluviums) and siderite (first time described in the Tamanduá River) in samples of white and brown clays, respectively, marks the spectral signature of these two clay classes. Of great interest is the fact that the presence (or absence), type and amount of impurities determined by RS in such clays showed a remarkable correlation with their application in the ceramic manufacturing industry. Therefore, in view of the exploratory nature of this research, the results using RS to characterize particular industry-aimed clays proved to be very promising.

References

Brindley, G.W., 1980. Quantitative X-ray Mineral Minerals and their X-ray Identification. In: Brindley, G.W., Brown, G. (Eds.), Mineralogical Society, London, pp. 411–438.

Brindley, G.W., Brown, G. (Eds.), 1984. Crystal Structures of Clay Minerals and their X-ray Identification. Monography, vol. 5. Mineralogical Society, London. 495 pp.

Clark, R.N., 1999. Spectroscopy of rocks and minerals, and principles of spectroscopy, chapter 1, In: Rencz, A.N. (Ed.), Remote Sensing for the Earth Sciences: Manual of Remote Sensing, 3 ed. John Wiley & Sons, Inc., New York, pp. 3–58. v.3.

Clark, R.N., Swayze, G.A., King, T.V.V., Calvin, W.M., 1993. Digital spectral library, version 1, 0.2 to 3.0 um. U.S. Geological Survey, Open File Report 93-592. 1326 pp.

Crowley, J.K., Vergo, N., 1988. Near-infrared reflectance spectra of mixtures of kaolin-group minerals; use in clay mineral studies. Clays and Clay Minerals 36 (4), 310–316.

Curtiss, B., Goetz, A.F.H., 1994. Field spectrometry: techniques and instrumentation. Proceedings of the International Symposium on Spectral Sensing Research, Boulder-Co, pp. 31–40.

Drury, S.A., 2001. Image Interpretation in Geology, 3 ed. London, London. 290 pp.

Ducart, D., Crosta, A.P., Souza Filho, C.R., Coniglio, J., 2006. Alteration mineralogy at the Cerro La Mina Epithermal Prospect, Patagonia, Argentina: field mapping, short-wave infrared spectroscopy, and ASTER Images. Economic Geology 101, 1010–1025.

Fortin, D., Leppard, G.G., Tessier, A., 1993. Characteristics of lacustrine diagenetic iron oxyhydroxides. Geochimica et Cosmochimica Acta 57 (18), 4391–4404.

Gaffey, S.J., 1987. Spectral reflectance of carbonate in the visible and near infrared (0.35–2.55 mm): anhydrous carbonate minerals. Journal of Geophysical Research 92 (B2), 1429–1440.

Gladwell, D.R., Lett, R.E., Laurence, P., 1983. Application of reflectance spectrometry to mineral exploration using portable radiometers. Economic Geology 78 (4), 699–710.

Goetz, A.F.H., Hauff, P., Shippert, M., 1991. Rapid detection and identification of OH-bearing minerals in the 0.9–1.0 mm region using a new portable field spectrometer. Thematic Conference on Geologic Remote Sensing, 8, Denver, Colorado, USA, Proceedings, pp. 1–11.

Guggenheim, S., Adams, J.M., Bain, D.C., Bergaya, F., Brigatti, M.F., Drits, V.A., Formoso, M.L.L., Galan, E., Kogure, T., Stanjek, H., 2006. Summary of recommendations of nomenclature committees relevant to clay mineralogy: report of the Association Internationale pour l'etude des Argiles (AIPEA) Nomenclature Committee for 2006. Clays and Clay Minerals 54, 761–772.

Hatchell, D.C., 1999. FieldSPec© Full Resolution-Technical Guide, 4th ed. Analytical Spectral Devices, Inc. (ASD), Boulder CO. 98 pp.

Hinckley, D.N., 1963. Variability in "crystallinity" values among the kaolin deposits of the Coastal Plain of Georgia and South Carolina. Clays and Clay Minerals 11, 229–235.

Hunt, G.R., 1977. Spectral signatures of particulate minerals in the visible and near infrared. Geophysics 42 (3), 501–513.

Hunt, G.R., 1980. Electromagnetic radiation, the communication link in remote sensing, chapter 2. In: Siegal, B.S., Gillespie, A.R. (Eds.), Remote Sensing in Geology. John Wiley & Sons, New York, pp. 5–45.

Hunt, G.R., Salisbury, J.W., 1971. Visible and near-infrared spectra of minerals and rocks: II-carbonates. Modern Geology 2, 23–30.

Kruse, F.A., 1997. Identification and mapping of minerals in drill core using hyperspectral image analysis of infrared reflectance spectra. International Journal of Remote Sensing 17 (9), 1623–1632.

Maracci, G., 1992. Field and Laboratory Narrow Band Spectrometers and the Techniques Employed, Chapter 3. In: Toselli, F., Bodechtel, J. (Eds.), Imaging Spectroscopy: Fundamentals and Prospective Applications. Klumer Academic Publishers, Netherlands, pp. 33–46.

Martinez-Alonso, S., Rustad, J., Goetz, A.F.H., 2002a. Ab initio quantum mechanical modeling of infrared vibrational frequencies of the OH group in dioctahedral phyllosilicates. Part I: methods, results and comparison to experimental data. American Mineralogist 87, 1215–1223.

Martinez-Alonso, S., Rustad, J., Goetz, A.F.H., 2002b. Ab initio quantum mechanical modeling of infrared vibrational frequencies of the OH group in dioctahedral phyllosilicates. Part II: main physical factors governing the OH vibrations. American Mineralogist 87, 1224–1234.

Meneses, R.M., Madeira Netto, J.S., 2001. Sensoriamento Remoto: Reflectância dos Alvos Naturais. Ed. UnB & Embrapa, Brasília. 262 pp.

Plançon, A., Giese, R.F., Snyder, R., 1988. The Hinckley Index for Kaolinites. Clay Minerals 23 (3), 249–260.

Pontual, S., Merry, N., Gamson, P., 1997. Spectral interpretation field manual, G-Max. Spectral Analysis Guides for Mineral Exploration. AusSpec Int. Pty.Ltd., Ferny Creek. v.1, 169 pp.

Pressinotti, M.M.N. 1991. Caracterização Geológica e Aspectos Genéticos dos Depósitos de Argilas Tipo "Ball Clay"de São Simão, SP. Unpublished MSc Thesis, Instituto de Geociências, Universidade de São Paulo, 141 pp.

Ruiz, M.S., 1990. Argilas-Perfil 4, capítulo IV. IPT-Instituto de Pesquisas Tecnológicas, Mercado Produtor Mineral do Estado de São Paulo-Levantamento e Análise. Pró-Minério-programa de Desenvolvimento de Recursos Minerais. São Paulo, pp. 61–86.

Sabins, F.F., 1999. Remote sensing for mineral exploration. Ore Geology Reviews 14, 157–183.

Sei, J., Touré, A.A., Olivier-Fourcade, J., Quiquampoix, H., Staunton, S., Jumas, J.C., Womes, M., 2004. Characterization of kaolinitic clays from the Ivory Coast (West Africa). Applied Clay Science 27, 235–239.

Santos, P.S., 1992. Ciência e Tecnologias de Argilas. Ed. Blücher Ltda, São Paulo, pp. 468–505. v.2.

Tanno, L.C., Motta, J.F.M., Cabral Jr., M., Kaseker, E.P., Pressinotti, M.M.N., 1994. Depósitos de Argilas para uso Cerâmico no Estado de São Paulo, cap.9. In: Schobbenhaus, C., Queiroz, E.T., Coelho, C.E.S. (Eds.), Principais Depósitos Minerais do Brasil-DNPM, Brasilia, v. IV-B-Rochas e Minerais Industriais, pp. 99–110.

Taylor, G.R., Reston, M., Hewson, R.D., 1997. An assessment of a portable spectrometer for analysis of geologial materials. Conference and Worshops os Applied Geologic Remote Sensing, 12, Denver, Colorado, Proceedings, part. II, pp. 409–416.

Townsend, T.E., 1987. Discrimination of iron alteration minerals in visible and near-infrared reflectance data. Journal of Geophysical Research 92 (B2), 1441–1454.

Turcq, B., Pressinotti, M.M.N., Martin, L., 1997. Paleohydrology and paleoclimate of the Past 33,000 years at the Tamanduá River, Central Brazil. Quaternary Research 47 (3), 284–294.

Whitney, G., Abrams, M.J., Goetz, A.F.H., 1983. Mineral discrimination using a portable ratio-determining radiometer. Economic Geology 78 (4), 688–698.

Wilson, I.R., 1983. Ball Clays inglesas-origens, propriedades e usos em cerâmica. Cerâmica 29 (165), 217–238.